Direct access to the moments of scattering distributions in x-ray imaging

Peter Modregger (iD), Marco Endrizzi (iD), and Alessandro Olivo

View Online   **Export Citation**   **CrossMark**

ARTICLES YOU MAY BE INTERESTED IN

AIP Publishing

Direct access to the moments of scattering distributions in x-ray imaging

Peter Modregger,[a)] Marco Endrizzi, and Alessandro Olivo

Department of Medical Physics and Bioengineering, University College London, Gower Street,
WC1E 6BT London, United Kingdom

The scattering signal obtained by phase-sensitive x-ray imaging methods provides complementary information about the sample on a scale smaller than the utilised pixels, which offers the potential for dose reduction by increasing pixel sizes. Deconvolution-based data analysis provides multiple scattering contrasts but suffers from time consuming data processing. Here, we propose a moment-based analysis that provides equivalent scattering contrasts while speeding up data analysis by almost three orders of magnitude. The availability of rapid data processing will be essential for applications that require instantaneous results such as medical diagnostics, production monitoring, and security screening. Further, we experimentally demonstrate that the additional scattering information provided by the moments with an order higher than two can be retrieved without increasing exposure time or dose. © 2018 Author(s). All article content, except where otherwise noted, is licensed under a Creative Commons Attribution (CC BY) license (http://creativecommons.org/licenses/by/4.0/). https://doi.org/10.1063/1.5054849

In the context of phase-sensitive x-ray imaging techniques, scattering refers to the contrast channel arising from sample inhomogeneities that are smaller than the utilised pixels. The utilisation of such sub-pixel signals allows for increasing the pixel size while maintaining the signal and simultaneously decreasing dose and/or scan times significantly. The sensitivity towards sub-pixel information has been established for different x-ray imaging methods, such as analyser-based imaging (ABI),[1,2] grating interferometry (GI),[3–5] speckle-based imaging,[6–8] and edge-illumination (EI).[9,10] The potential of x-ray scattering is investigated for mammography,[10–12] bone structure determination,[13] and the diagnosis of several pulmonary diseases in both small[14–16] and large animals.[17]

Commonly used data analysis procedures provide a single contrast related to sub-pixel information, which is called the dark-field[3] or the scattering signal.[10] An alternative deconvolution-based approach that provides multiple and complementary scattering contrasts was originally developed for GI[18] and extended to tomography[19] and recently translated to EI.[20] In some applications, it was shown that deconvolution can provide a higher contrast to noise ratio and improved dose efficiency.[21,22] It was also demonstrated that the complementary contrasts can be exploited for quantitative imaging[23] without the need for additional scans required by other approaches.[5,24,25] While the deconvolution-based analysis is suitable for ABI, GI, and EI, the approach proposed below is not directly applicable to GI due to the sinusoidal nature of the provided signal. Thus, we will introduce the approach for EI and note that all results are directly applicable to ABI.

EI is a non-interferometric, phase-sensitive x-ray imaging technique that uses a pair of apertured masks (Fig. 1). The pre-sample mask confines the incident x-rays into smaller beamlets, which are broadened by the sample due to

scattering. The broadening is transformed into a detectable intensity variation by the detector mask that features apertures covering most of the detector pixels. The comparably large structure sizes of the optical elements (typically tens of microns) allow for simple mask fabrication[23] and render EI robust against vibrations and thermal variations. EI is readily compatible with laboratory-based x-ray tubes due to the achromaticity of the optical elements and the entire x-ray spectrum contributes to the signal.[26,27]

Accessing multiple scattering contrasts by deconvolution is based on the following approach. Scanning the pre-sample masks laterally by a fraction of its period provides a Gaussian-like intensity curve in each detector pixel. Repeating the scan with and without the sample yields the signals $s(\alpha)$ and $f(\alpha)$, respectively. Here, the scattering angle α is defined in a plane perpendicular to the line apertures of the utilised mask (Fig. 1). Scattering in the orthogonal direction does not change the detectable signal and, thus, can be omitted for the rest of the discussion. The angularly resolved scattering distribution $g(\alpha)$, which represents the sample's scattering signal within one pixel, is then implicitly defined by[9,10,20,28,29]

$$s(\alpha) = f(\alpha) \otimes g(\alpha), \tag{1}$$

where $\otimes$ denotes the convolution operator. The scattering distribution $g(\alpha)$ can be accessed from experimental data by deconvolving $s(\alpha)$ with $f(\alpha)$ and iterative Lucy-Richardson deconvolution[30,31] has been established as a reliable method.[20,21] The kth iteration step of the deconvolution is performed by computing

$$g^{k+1} = g^k \times \left(\frac{s}{g^k \otimes f} \otimes \bar{\bar{f}} \right), \tag{2}$$

where $\bar{\bar{f}}$ denotes f mirrored at the origin. Usually, the sample signal is chosen as the starting value: $g^0 = s$. Lucy-Richardson deconvolution features an implicit positive
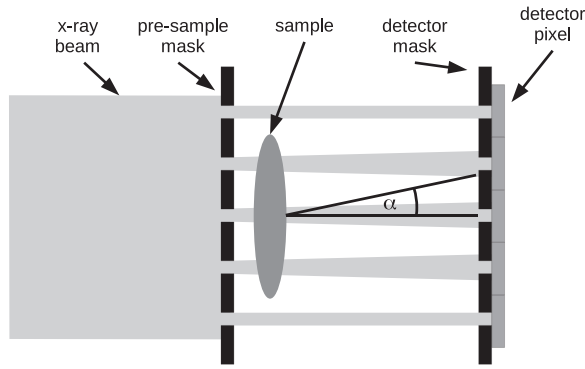
[a)]Electronic mail: p.modregger@ucl.ac.uk

FIG. 1. Setup for x-ray imaging based on edge-illumination. The scattering angle α is given by the geometry of the setup.

constraint and is guaranteed to converge to the maximum likelihood solution if the experimental noise is given by Poisson statistics, which is commonly the case in x-ray imaging.[32,33]

In order to retrieve multiple contrasts relating to the shape of g, a moment analysis can be applied to the scattering distributions. Depending on normalisation and centralisation, different definitions of the moments need to be distinguished. The un-normalised, un-centralised moments of an arbitrary function $h(\alpha)$ are given by

$$M_n(h) = \int \alpha^n h(\alpha)\, d\alpha, \tag{3}$$

where n is an integer denoting the order of the moment. Dividing by M_0 yields the normalised, un-centralised moments

$$\bar{M}_n(h) = M_n/M_0 \quad \text{for } n \geq 1, \tag{4}$$

and shifting by $\bar{M}_1$ leads to the normalised, centralised moments

$$\tilde{M}_n(h) = \int (\alpha - \bar{M}_1)^n h(\alpha)\, d\alpha / M_0 \quad \text{for } n \geq 2. \tag{5}$$

It has been experimentally demonstrated that the first moment of the scattering distribution $M_0(g)$ corresponds to absorption, $\bar{M}_1(g)$ to the differential phase signal, and $\tilde{M}_2(g)$ to scattering strength.[20] The relation of these moments to sample properties is provided in Ref. 23.

Given typical noise levels in experiments, about 1000 iterations steps are required to ensure convergence of the Lucy-Richardson deconvolution, which may lead to cumbersome data processing times. For example, data processing of the dragon fly in Ref. 20 took around 1 h for a 400×300 pixel field of view on a standard desktop PC. This renders iterative deconvolution unsuitable for time sensitive applications.

Therefore, we propose an alternative data analysis approach that uses the known moments of convolutions,[34] the derivation of which is briefly sketched in the following. The moments defined in Eq. (3) appear as derivatives at zero frequencies in Fourier space[35]

$$M_n(s) = \frac{\sqrt{2\pi}}{(-i)^n} \frac{d^n \hat{s}}{dq^n}\bigg|_{q=0}, \tag{6}$$

where the symbol $\hat{\ }$ denotes the Fourier transform and q the variable in Fourier space. Since s is given by a convolution, its Fourier transform corresponds to a product

$$s = f \otimes g \Longleftrightarrow \hat{s} = \sqrt{2\pi}\, \hat{f} \times \hat{g}. \tag{7}$$

Inserting Eq. (7) into Eq. (6) and dividing by M_0 lead to

$$\bar{M}_n(s) = \sum_{k=0}^{n} \binom{n}{k} \bar{M}_k(f)\, \bar{M}_{n-k}(g), \tag{8}$$

with the binomial coefficient $\binom{n}{k}$. Similar equations hold true for the normalised, centralised moments $\tilde{M}_n$,[34] which can be solved for the moments of g. The result for the first five moments is

$$M_0(g) = M_0(s)/M_0(f), \tag{9}$$

$$\bar{M}_1(g) = \bar{M}_1(s) - \bar{M}_1(f), \tag{10}$$

$$\tilde{M}_2(g) = \tilde{M}_2(s) - \tilde{M}_2(f), \tag{11}$$

$$\tilde{M}_3(g) = \tilde{M}_3(s) - \tilde{M}_3(f), \tag{12}$$

$$\tilde{M}_4(g) = \tilde{M}_4(s) - \tilde{M}_4(f) - 6\tilde{M}_2(f)\tilde{M}_2(g). \tag{13}$$

First moment terms do not appear in equations with $n > 1$ because $\tilde{M}_1 = 0$. For the scattering width $\tilde{M}_2$, the above equation is in agreement with published results.[36] Since the moments of s and f can be directly calculated from experimental data, Eqs. (9)–(13) provide direct access to the moments of the scattering distribution g without the need for time consuming iterative deconvolution.

In order to experimentally compare the results of deconvolution and direct moment analysis, we used an EI-based imaging system at University College London. A Rigaku MM007 rotating anode with a Mo target was used as an x-ray source and operated at a 25 mA current and a 40 kVp voltage. The pre-sample mask consisted of a series of Au lines on a graphite substrate with a pitch of 79 μm and an opening of 10 μm, while the detector mask had a pitch of 98 μm and an opening of 17 μm. Both masks were manufactured by Creatv Microtech (Potomac, MD). The x-ray detector was a Hamamatsu C9732DK flat panel sensor featuring a binned pixel size of 100 μm. The sample to detector distance was 0.32 m, and the total setup length was 2 m.

The sample was a dragon fly, which was known to provide a sufficient signal for the first five moments. The sample mask was scanned over one pitch with 32 steps and an exposure time of 25 s per step. The same dataset was used for the deconvolution [Eq. (2)] and moment analysis (Eqs. 9–13). The resulting scattering contrasts (Fig. 2) show an excellent visual agreement between the two approaches, while data processing for direct moment analysis was about 600 times faster than for deconvolution. Furthermore, direct moment analysis eliminates the number of iteration steps as a necessary parameter for deconvolution.

Table I presents a performance comparison of deconvolution and moment analysis. The high degree of visual agreement between the approaches is confirmed by the correlation factors (≥ 0.9 for all contrasts). Columns 3 and 4 compare the standard deviation of the signals in a 50×50 pixel
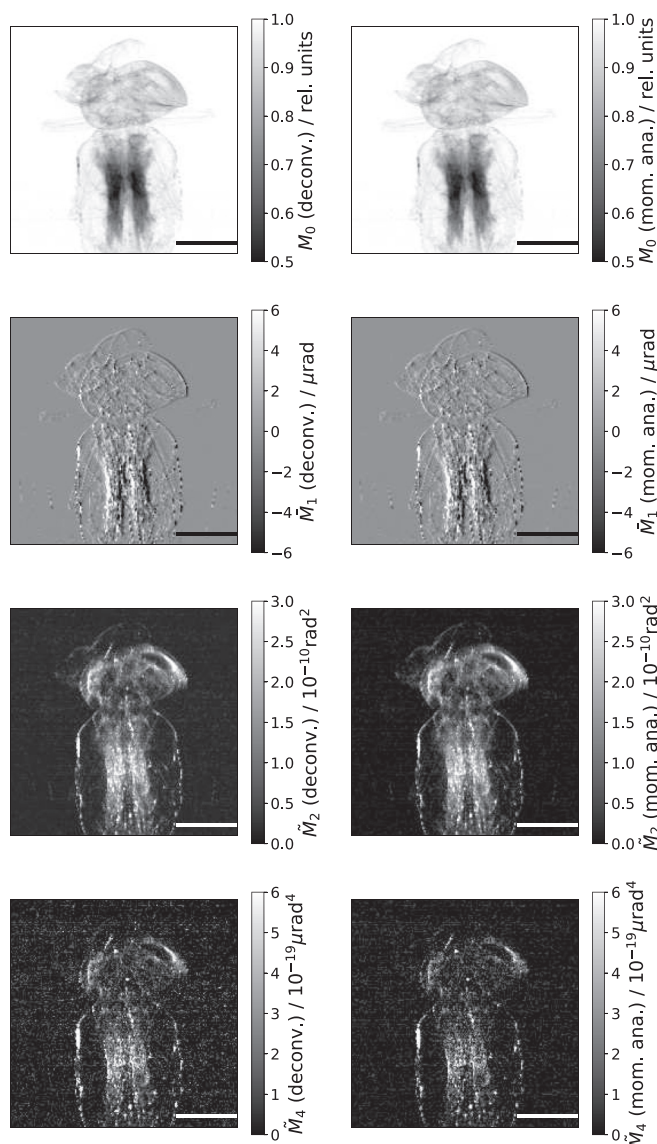
FIG. 2. Comparison of four moments retrieved by deconvolution (left column) and moment analysis (right column). The sample was a dragon fly and the two data analysis approaches deliver practically identical results. The pixel size is $100\,\mu$m, and scale bars are 5 mm.

background area as a measure of the noise level in the two analysis approaches. With the exception of $\tilde{M}_2$ (details discussed below), both approaches deliver similar noise levels.

TABLE I. Performance comparison of the two data analysis approaches for the first five moments shown in Fig. 2. 2nd column: correlation between the results of deconvolution and moment analysis. 3rd and 4th columns: standard deviation of the signals in the background. The additional entry for $\tilde{M}_2$ relates to the standard deviation of larger scattering values (see the text for explanation).

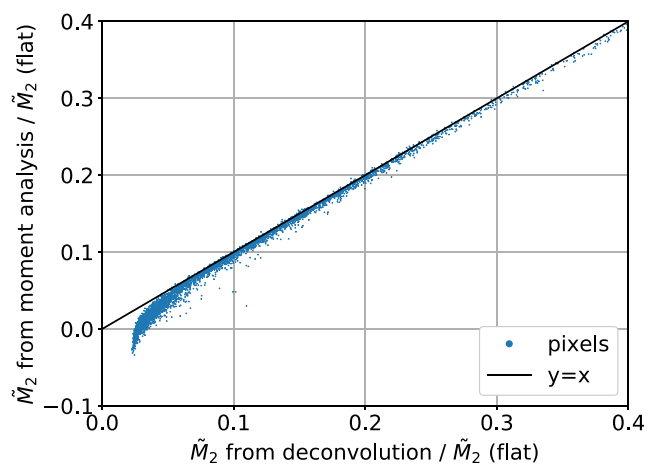|	Correlation	Std. deconv.	Std. mom. ana.
M_0	1.00	2.6×10^{-3}	2.6×10^{-3}
$\bar{M}_1$	0.99	6.4×10^{-8} rad	6.5×10^{-8} rad
$\tilde{M}_2$	0.99	4.6×10^{-12} rad^2	8.3×10^{-12} rad^2
		$(6.7 \times 10^{-11}$ rad$^2)$	$(6.7 \times 10^{-11}$ rad$^2)$
$\tilde{M}_3$	0.90	3.3×10^{-16} rad^3	3.1×10^{-16} rad^3
$\tilde{M}_4$	0.90	4.5×10^{-20} rad^4	4.4×10^{-20} rad^4

FIG. 3. Scatter plot of $\tilde{M}_2$ as retrieved by deconvolution and moment analysis. The $\tilde{M}_2$ values have been normalised by the mean of $\tilde{M}_2$ in the flat scan ($\tilde{M}_2(f) = 7 \times 10^{-10}$ rad^2). For small values of $\tilde{M}_2(g)$, there is a noticeable discrepancy between the results of the algorithms, which is due to the inability of the deconvolution approach to retrieve a scattering distribution with zero width in the presence of noise.

For the 2nd moment, the scatter plot of values retrieved by deconvolution and moment analysis (Fig. 3) reveals a discrepancy for scattering strengths that are small compared to the width of the flat-field scan ($\tilde{M}_2(g) \leq 0.05 \times \tilde{M}_2(f)$). In this case, the deconvolution approach [Eq. (2)] does not retrieve the correct δ-shaped signal for g due to the presence of noise,[22] but will retrieve a signal with $\tilde{M}_2(g) > 0$. The moment analysis, on the other hand, is not subject to such a restriction. The difference in bias between the two approaches is also reflected in the mean of the background areas, which are $\tilde{M}_2 = 2.1 \times 10^{-11}$ rad^2 for deconvolution and $\tilde{M}_2 = 2.8 \times 10^{-12}$ rad^2 and, thus, an order of magnitude smaller for direct moment analysis. However, Table I shows that deconvolution provides $\tilde{M}_2$ values with a smaller standard deviation than moment analysis in the background area. Nevertheless, moment analysis would be the preferred option for quantitative data analysis. For large scattering values ($\tilde{M}_2(g) \geq 0.1 \times \tilde{M}_2(f)$), the two approaches deliver the same sensitivity (bracketed entries for $\tilde{M}_2$ in Table I).

Finally, we investigated the influence of the acquired number of sample points on the functions $s(\alpha)$ and $f(\alpha)$ (i.e., number of images per scan). Since at least $n+1$ scan points are required for the linear independence of nth moment, increasing the number of scan points increases the number of accessible and complementary scattering information.

To this end, we acquired an additional dataset, where we varied the number of scan points from 5 to 11, while keeping the total exposure time constant (200 s). We used the standard deviation of the different scattering contrasts in a background area retrieved by direct moment analysis to quantify the dependency. As can be seen in Fig. 4, the noise levels vary within a small 15% interval, which implies that the sensitivity of the different contrasts does not change significantly with the number of scan points. In essence, this means that moment analysis provides the additional scattering contrasts (i.e., moments with order higher than 2) without the need to increase total exposure time or dose.

In conclusion, we have established a direct moment analysis as an alternative approach for retrieving multiple
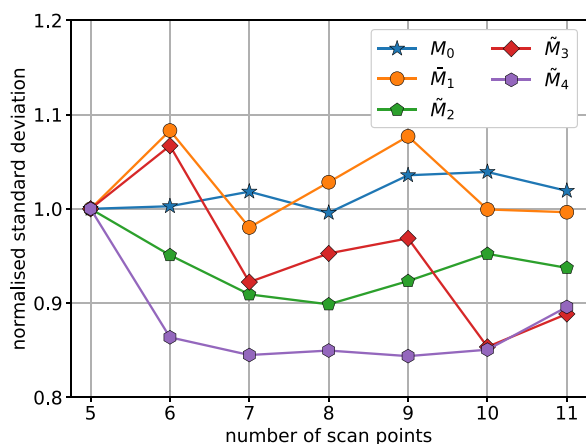
FIG. 4. Standard deviations of the moment values in the background as a function of the number of scan points with constant total exposure time. The values have been normalised by the value corresponding to five scan points, which is the smallest possible number for five linear independent moments.

scattering contrasts for EI. We also suggest that this approach can be readily extended to ABI. Direct moment analysis delivers results equivalent to previously utilised deconvolution, while speeding up data processing by almost three orders of magnitude and providing unbiased values for small or absent scattering signals. Furthermore, we have experimentally demonstrated that increasing the number of scan points while keeping total exposure time and dose constant provides additional scattering information without losing sensitivity. Fast data processing that provides reliable scattering contrasts will be crucial for applications demanding rapid feedback, such as medical diagnostics, production monitoring, and security screening.

See supplementary material for the implementation of data analysis in Python.

[1]L. Rigon, H.-J. Besch, F. Arfelli, R.-H. Menk, G. Heitner, and H. Plothow-Besch, J. Phys. D: Appl. Phys. 36, A107 (2003).
[2]H. Suhonen, M. Fernández, A. Bravin, J. Keyrilainen, and P. Suortti, J. Synchrotron Radiat. 14, 512 (2007).
[3]F. Pfeiffer, M. Bech, O. Bunk, P. Kraft, E. F. Eikenberry, and C. David, Nat. Mater. 7, 134 (2008).
[4]W. Yashiro, Y. Terui, K. Kawabata, and A. Momose, Opt. Express 18, 16890 (2010).
[5]S. K. Lynch, V. Pai, J. Auxier, A. F. Stein, E. E. Bennett, C. K. Kemble, X. Xiao, W.-K. Lee, N. Y. Morgan, and H. Wen, Appl. Opt. 50, 4310 (2011).
[6]K. S. Morgan, P. Modregger, S. C. Irvine, S. Rutishauser, V. A. Guzenko, M. Stampanoni, and C. David, Opt. Lett. 38, 4605 (2013).
[7]I. Zanette, T. Zhou, A. Burvall, U. Lundström, D. H. Larsson, M. Zdora, P. Thibault, F. Pfeiffer, and H. M. Hertz, Phys. Rev. Lett. 112, 253903 (2014).
[8]H. Wang, Y. Kashyap, and K. Sawhney, Phys. Rev. Lett. 114, 103901 (2015).
[9]M. Endrizzi and A. Olivo, J. Phys. D: Appl. Phys. 47, 505102 (2014).
[10]M. Endrizzi, P. C. Diemoz, T. P. Millard, J. Louise Jones, R. D. Speller, I. K. Robinson, and A. Olivo, Appl. Phys. Lett. 104, 024106 (2014).
[11]M. Stampanoni, Z. Wang, and T. Thüring, Invest. Radiol. 46, 801 (2011).
[12]Z. Wang, N. Hauser, G. Singer, M. Trippel, R. A. Kubik-Huch, C. W. Schneider, and M. Stampanoni, Nat. Commun. 5, 3797 (2014).
[13]H. Wen, E. E. Bennett, M. M. Hegedus, and S. Rapacchi, Radiology 251, 910 (2009).
[14]A. Yaroshenko, F. G. Meinel, M. Bech, A. Tapfer, A. Velroyen, S. Schleede, S. D. Auweter, A. Bohla, A. Ö. Yildirim, K. Nikolaou, F. Bamberg, O. Eickelberg, M. F. Reiser, and F. Pfeiffer, Radiology 269, 427 (2013).
[15]F. G. Meinel, A. Yaroshenko, K. Hellbach, M. Bech, A. Velroyen, F. Bamberg, O. Eickelberg, K. Nikolaou, F. Maximilian, F. Pfeiffer, and O. Ali, Invest. Radiol. 49, 653 (2014).
[16]K. Scherer, A. Yaroshenko, D. A. Bölükbas, L. B. Gromann, K. Hellbach, F. G. Meinel, M. Braunagel, J. von Berg, O. Eickelberg, M. F. Reiser, F. Pfeiffer, S. Meiners, and J. Herzen, Sci. Rep. 7, 402 (2017).
[17]L. B. Gromann, F. De Marco, K. Willer, P. B. Noël, K. Scherer, B. Renger, B. Gleich, K. Achterhold, A. A. Fingerle, D. Muenzel, S. Auweter, K. Hellbach, M. Reiser, A. Baehr, M. Dmochewitz, T. J. Schroeter, F. J. Koch, P. Meyer, D. Kunka, J. Mohr, A. Yaroshenko, H.-I. Maack, T. Pralow, H. van der Heijden, R. Proksa, T. Koehler, N. Wieberneit, K. Rindt, E. J. Rummeny, F. Pfeiffer, and J. Herzen, Sci. Rep. 7, 4807 (2017).
[18]P. Modregger, F. Scattarella, B. R. Pinzer, C. David, R. Bellotti, and M. Stampanoni, Phys. Rev. Lett. 108, 048101 (2012).
[19]P. Modregger, M. Kagias, S. Peter, M. Abis, V. A. Guzenko, C. David, and M. Stampanoni, Phys. Rev. Lett. 113, 020801 (2014).
[20]P. Modregger, T. P. Cremona, C. Benarafa, J. C. Schittny, A. Olivo, and M. Endrizzi, Sci. Rep. 6, 30940 (2016).
[21]T. Weber, G. Pelzer, F. Bayer, F. Horn, J. Rieger, A. Ritter, A. Zang, J. Durst, G. Anton, and T. Michel, Opt. Express 21, 18011 (2013).
[22]F. Horn, F. Bayer, G. Pelzer, J. Rieger, A. Ritter, T. Weber, A. Zang, T. Michel, and G. Anton, SPIE Proc. 9033, 903351 (2014).
[23]P. Modregger, M. Kagias, S. C. Irvine, R. Brönnimann, K. Jefimovs, M. Endrizzi, and A. Olivo, Phys. Rev. Lett. 118, 265501 (2017).
[24]S. Gkoumas, P. Villanueva-Perez, Z. Wang, L. Romano, M. Abis, and M. Stampanoni, Sci. Rep. 6, 35259 (2016).
[25]R. P. Harti, M. Strobl, B. Betz, K. Jefimovs, M. Kagias, and C. Grünzweig, Sci. Rep. 7, 44588 (2017).
[26]P. R. T. Munro, K. Ignatyev, R. D. Speller, and A. Olivo, Opt. Express 18, 19681 (2010).
[27]M. Endrizzi, F. A. Vittoria, G. Kallon, D. Basta, P. C. Diemoz, A. Vincenzi, P. Delogu, R. Bellazzini, and A. Olivo, Opt. Express 23, 16473 (2015).
[28]P. Modregger, D. Lübbert, P. Schäfer, and R. Köhler, Phys. Rev. B 74, 054107 (2006).
[29]Z. Wang, K.-J. Kang, Z.-F. Huang, and Z.-Q. Chen, Appl. Phys. Lett. 95, 094105 (2009).
[30]W. Richardson, J. Opt. Soc. Am. 62, 55 (1972).
[31]L. B. Lucy, Astron. J. 79, 745 (1974).
[32]V. Revol, C. Kottler, R. Kaufmann, U. Straumann, and C. Urban, Rev. Sci. Instrum. 81, 073709 (2010).
[33]P. Modregger, B. R. Pinzer, T. Thüring, S. Rutishauser, C. David, and M. Stampanoni, Opt. Express 19, 18324 (2011).
[34]C. Laury-Micoulaut, Astron. Astrophys. 51, 343 (1976).
[35]F. James, Statistical Methods in Experimental Physics, 2nd ed. (World Scientific Publishing Co. Pte. Ltd., Singapore, 2006).
[36]M. Endrizzi, F. A. Vittoria, L. Rigon, D. Dreossi, F. Iacoviello, P. Shearing, and A. Olivo, Phys. Rev. Lett. 118, 243902 (2017).